Journal of Statistical Mechanics: Theory and Experiment
An IOP and SISSA journal

Combustion simulation via lattice Boltzmann and reduced chemical kinetics

Eliodoro Chiavazzo[1], Iliya V Karlin[1], Alexander N Gorban[2] and Konstantinos Boulouchos[1]

[1] Aerothermochemistry and Combustion Systems Laboratory (LAV), Swiss Federal Institute of Technology (ETH), 8092 Zurich, Switzerland
[2] Department of Mathematics, University of Leicester, Leicester LE1 7RH, UK
E-mail: chiavazzo@lav.mavt.ethz.ch, karlin@lav.mavt.ethz.ch, ag153@leicester.ac.uk and boulouchos@lav.mavt.ethz.ch

Received 28 October 2008
Accepted 16 February 2009
Published 16 June 2009

Online at stacks.iop.org/JSTAT/2009/P06013
doi:10.1088/1742-5468/2009/06/P06013

Abstract. In this work, we present and validate a methodology for coupling reduced models of detailed combustion mechanisms within the lattice Boltzmann framework. A detailed mechanism (9 species, 21 elementary reactions) for modeling reacting mixtures of air and hydrogen is considered and reduced using the method of invariant grids (MIG). In particular, a 2D quasi-equilibrium grid is constructed, further refined via the MIG method, stored in the form of tables and used to simulate a 1D flame propagating freely through a homogeneous premixed mixture. Comparisons between the detailed and reduced models show that the technique presented enables one to achieve a remarkable speedup in the computations with excellent accuracy.

Keywords: chemical kinetics, combustion, lattice Boltzmann methods

J. Stat. Mech. (2009) P06013

1742-5468/09/P06013+22$30.00

Contents

1. Introduction

The numerical solution of the full set of governing equations, as dictated by modeling of reactive flows with detailed chemical kinetics, remains a challenging task. The reasons are as follows. On one hand, there are a large number of conservation equations to be solved in order to keep track of each chemical species. On the other hand, the reaction mechanism introduces large differences in the time scales of species dynamics, and the numerical implementation has to cope with *stiffness*. The latter aspect has a particularly negative impact on the explicit schemes, such as the lattice Boltzmann method, where reducing the time step becomes necessary in order to avoid numerical instabilities. As a result, the smallest time scales need to be resolved even when one is interested only in the slow dynamics. In addition, the larger the number of elementary reactions involved in the detailed mechanism, the more significant the computational effort, due to the evaluation of reaction rates.

J. Stat. Mech. (2009) P06013

In contrast, the disparate time scales can be exploited in order to construct a reduced description of the detailed model. For instance, because of the stiffness, the dynamics of homogeneous reactive systems is often characterized by a short transient towards a low dimensional manifold in the concentration space, known as the *slow invariant manifold*. The subsequent dynamics is slower and it proceeds along the manifold itself, until a steady state is reached. Constructing such manifolds can lead to a simpler and less stiff description of the reactive system; moreover, the interesting slow dynamics can still be reproduced with high accuracy. Therefore, much effort has been devoted to achieving that aim; the method of invariant grids (MIG) [4], the intrinsic low dimensional manifold (ILDM) approach [14] and the computational singular perturbation (CSP) method [15] are representative examples. The present study intends to investigate the potential of using reduced kinetics within the lattice Boltzmann framework: to this end, here we use a reduced description (two degrees of freedom) of a detailed mechanism for reactive mixing of hydrogen and air, obtained by the MIG.

The paper is organized as follows. In section 2, we briefly review some basics of reaction kinetics and thermodynamic Lyapunov functions for closed dissipative systems. For illustration purposes, a one-dimensional reduced description of a simple chain branching mechanism with two degrees of freedom is discussed in section 3. In section 4, the implementation of the method of invariant grids is reviewed. The detailed lattice Boltzmann scheme for simulating reactive flows and the suggested coupling with reduced chemistry are presented in section 5. The validation study is presented in section 6, where we consider the propagation of a flame front in a premixed mixture of hydrogen and air. Finally, conclusions are drawn in section 7.

2. Theoretical background

2.1. Detailed reaction kinetics

Let $x_1, \ldots, x_n$ be n chemical species participating in a complex reaction mechanism with r reversible steps,

$$\alpha_{s1}x_1 + \cdots + \alpha_{sn}x_n \rightleftharpoons \beta_{s1}x_1 + \cdots + \beta_{sn}x_n, \quad s = 1, \ldots, r, \tag{1}$$

where α_{si} and β_{si} are stoichiometric coefficients of species i in the reaction step s for reactants and products, respectively. Let the stoichiometric vectors be $\boldsymbol{\alpha}_s = (\alpha_{s1}, \ldots, \alpha_{sn})$, $\boldsymbol{\beta}_s = (\beta_{s1}, \ldots, \beta_{sn})$ and $\boldsymbol{\gamma}_s = \boldsymbol{\beta}_s - \boldsymbol{\alpha}_s$. The reaction rate of step s is given by the mass action law:

$$\Omega_s = \Omega_s^+ - \Omega_s^-, \qquad \Omega_s^+ = k_s^+(T) \prod_{i=1}^{n} [X_i]^{\alpha_i}, \qquad \Omega_s^- = k_s^-(T) \prod_{i=1}^{n} [X_i]^{\beta_i}, \tag{2}$$

where $[X_i]$ is the molar concentration of species i. The forward and the reverse reaction rate constants k_s^+, k_s^- take on the Arrhenius form

$$k_s(T) = A_s T^{\beta_s} \exp\left(\frac{-E_{\mathrm{as}}}{RT}\right), \tag{3}$$

where A_s denotes the pre-exponential factor, β_s the temperature exponent, and E_{as} is the activation energy of reaction s. The rate of change of species i is given by

$$\dot{\omega}_i = \sum_{s=1}^{r} \boldsymbol{\gamma}_s (i)\, \Omega_s, \tag{4}$$

with forward and reverse reaction rate constants related by the equilibrium constant $K_{c,s} = k_s^+ / k_s^-$. A detailed discussion of the theory of chemical kinetics can be found in, e.g., the classical work of Williams [1].

In the following, we focus on ideal gas mixtures in closed adiabatic reactors with fixed total pressure p and averaged specific enthalpy $\bar{h}$. In this case, any state of the reacting mixture is fully described by the vector $\boldsymbol{\psi} = (p, \bar{h}, Y_1, \ldots, Y_n)^{\mathrm{T}}$ whose temporal evolution obeys a set of ordinary differential equations (ODEs):

$$\frac{\mathrm{d}\boldsymbol{\psi}}{\mathrm{d}t} = \left(0, 0, \frac{\dot{\omega}_1 W_1}{\bar{\rho}}, \ldots, \frac{\dot{\omega}_n W_n}{\bar{\rho}}\right)^{\mathrm{T}}, \tag{5}$$

where the superscript $^{\mathrm{T}}$ denotes transposition, Y_i and W_i are the mass fraction and molecular weight of species i, respectively. The mixture enthalpy $\bar{h}$ and density $\bar{\rho}$ can be explicitly written as

$$\bar{h} = \sum_{i=1}^{n} h_i (T)\, Y_i, \qquad \bar{\rho} = \sum_{i=1}^{n} W_i [X_i]. \tag{6}$$

Like in CHEMKIN [2], for any species i, the dependence of the specific enthalpy h_i on temperature T (in kelvins) is represented by a polynomial fit

$$h_i (T) = RT \left(a_{i1} + \frac{a_{i2}}{2} T + \frac{a_{i3}}{3} T^2 + \frac{a_{i4}}{4} T^3 + \frac{a_{i5}}{5} T^4 + \frac{a_{i6}}{T}\right). \tag{7}$$

Here, R denotes the universal gas constant while the coefficients a_{ij} are tabulated constants. It is worth noting that the temperature T, corresponding to the state $\boldsymbol{\psi}$, is not explicitly known. Therefore, the evaluation of the right-hand side of (5) is obtained after computing T via iterative solution of the first equation in (6).

2.2. Thermodynamic Lyapunov function

Equation (5) describes the temporal evolution of an adiabatic batch reactor towards a unique steady state. Due to the second law of thermodynamics, the specific mixture-averaged entropy (in mass units) $\bar{s}$ of such a reactor monotonically increases, starting from any initial non-equilibrium condition. In other words, since the function $\tilde{G} = -\bar{s}$ only depends on the state $\boldsymbol{\psi}$ and must monotonically decrease in time under the dynamics of (5), it is a Lyapunov function of the system (5). For an ideal gas mixture, $\tilde{G}$ takes the explicit form

$$\tilde{G} = -\bar{s} = \frac{-\sum_{i=1}^{n} \left[s_i (T) - R \ln (X_i) - R \ln (p/p_{\mathrm{ref}})\right] X_i}{\bar{W}}, \tag{8}$$

where $\bar{W} = \sum_{i=1}^{n} W_i X_i$, p_{ref}, X_i and s_i are the mixture molecular weight, a given reference pressure, the mole fraction and the specific entropy (in molar units) of species

J. Stat. Mech. (2009) P06013

i, respectively. The specific entropy s_i, according to [2], is assumed to have the following dependence on the temperature T:

$$s_i(T) = R\left(a_{i1}\ln T + a_{i2}T + \frac{a_{i3}}{2}T^2 + \frac{a_{i4}}{3}T^3 + \frac{a_{i5}}{4}T^4 + a_{i7}\right). \tag{9}$$

Let d be the number of chemical elements involved in the reaction. Let μ_{ik} be the number of atoms of the k th element in species i. Another form of the Lyapunov function of (5) can be constructed as follows:

$$G = \tilde{G} + \sum_{k=1}^{d}\left(\lambda_k \sum_{i=1}^{n}\frac{\mu_{ik}}{W_i}Y_i\right), \tag{10}$$

where the Lagrange multipliers λ_k are chosen in such a way that $\boldsymbol{\nabla} G|_{p,\bar{h}} = \mathbf{0}$ at the steady state, with the gradient of G computed for fixed p and $\bar{h}$. Because of the conservation of atoms, the time derivative of (10) is non-positive:

$$\frac{\mathrm{d}G}{\mathrm{d}t} = \frac{\mathrm{d}\tilde{G}}{\mathrm{d}t} \leq 0, \qquad \frac{\mathrm{d}N_k}{\mathrm{d}t} = 0, \tag{11}$$

with the conserved atom mole numbers N_k expressed as

$$N_k = \sum_{i=1}^{n}\frac{\mu_{ik}}{W_i}Y_i, \qquad k = 1,\ldots,d. \tag{12}$$

3. Example: a chain branching model

To gain a better understanding of some notions discussed later on in the paper, we consider here a simple kinetic model adopted to illustrate isothermal chain branching mechanisms. It consists of three species x_1, x_2 and x_3 involved in the following three reactions:

$$\begin{array}{ll}(1) & x_1 \rightarrow x_2,\\ (2) & x_1 + x_2 \rightarrow x_3 + \lambda x_2,\\ (3) & x_2 \rightarrow x_3,\end{array} \tag{13}$$

known as initiation, propagation and termination steps, respectively. The compounds x_1, x_2 and x_3 are representative of a reactant, a chain carrier and a product, respectively, with λ denoting a positive chain branching constant. Let k_i^+, k_p^+ and k_t^+ be the forward reaction rate constants of the three steps (13); the time evolution of the x_1 and x_2 molar concentrations obeys the following system:

$$\begin{aligned}\frac{\mathrm{d}[X_1]}{\mathrm{d}t'} &= -k_i^+[X_1] - k_p^+[X_1][X_2],\\ \frac{\mathrm{d}[X_2]}{\mathrm{d}t'} &= k_i^+[X_1] + k_p^+(\lambda-1)[X_1][X_2] - k_t^+[X_2].\end{aligned} \tag{14}$$

Introducing the dimensionless variables $z = [X_1]/[X_1^0]$, $y = k_p^+[X_2]/k_i^+$, $t = k_i^+ t'$ and the parameters $\varepsilon = k_i^+[X_1^0]/k_p^+$, $\varphi = k_t^+[X_1^0]/k_p^+$ with $[X_1^0]$ denoting a reference concentration, the rate equations (14) attain a non-dimensional form:

$$\frac{\mathrm{d}z}{\mathrm{d}t} = -z - zy = f_z, \qquad \frac{\mathrm{d}y}{\mathrm{d}t} = \frac{1}{\varepsilon}[z + (\lambda-1)zy - \varphi y] = f_y. \tag{15}$$

J. Stat. Mech. (2009) P06013

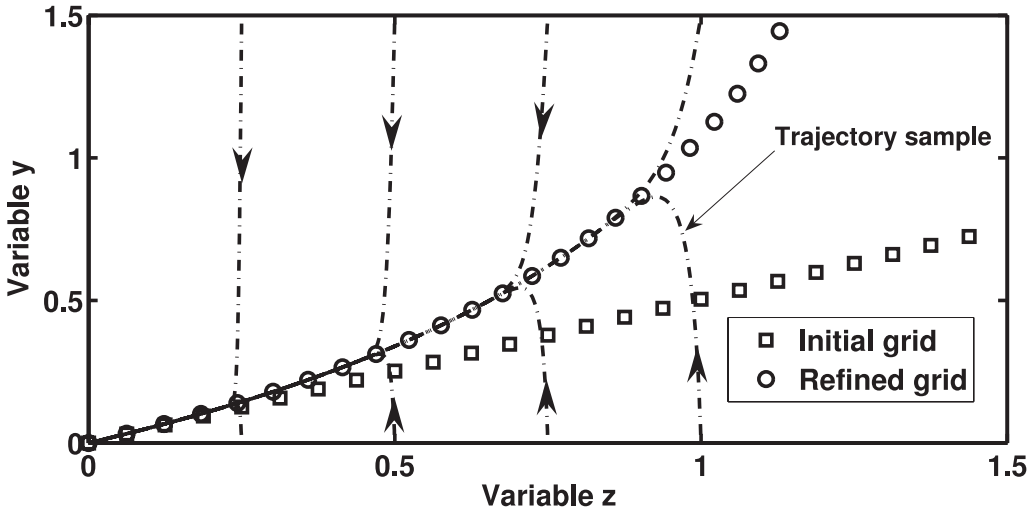

Figure 1. Several solution trajectories of (15) in the space (z, y) with $\varepsilon = 0.015$, $\lambda = \varphi = 2$.

The system (15) has a single steady state at $(z, y) = (0, 0)$. On choosing $\varepsilon \ll 1$, the propagation step occurs at a faster rate than the initiation step, and the above becomes a *stiff* planar system. As a result, typical solution trajectories in the phase space (z, y), starting from arbitrary initial conditions, quickly approach a one-dimensional attractor, and afterwards keep moving along it towards the steady state at a slower rate. Figure 1 shows the case corresponding to $\varepsilon = 0.015$ and $\lambda = \varphi = 2$. In the following, we refer to such attractors as invariant manifolds of the slow motions, or *slow invariant manifolds* (SIM) for short.

3.1. Invariant grid construction

Although the system (15) possesses two degrees of freedom, a one-dimensional description of it can be attained by extracting the asymptotic slow dynamics, which takes place along the slow invariant manifold. Therefore, constructing SIM represents a general and automated approach when seeking for a reduced model of reaction mechanisms. In this work, manifolds are represented by discrete collections of points in the phase space which are named *grids*. Accurate discrete descriptions of slow invariant manifolds are termed *invariant grids*, and are computed using the method of invariant grids (MIG).

For illustration purposes, the construction of a one-dimensional reduced description of (15), under the conditions of figure 1, is discussed below. The method of invariant grids is an iterative procedure, which aims at constructing the invariant grid by subsequent refinements from an initial approximation (*initial grid*). The eigenvector of the first-derivative matrix $\boldsymbol{J}$ (Jacobian) of (15)

$$\boldsymbol{J} = \begin{bmatrix} \partial f_z/\partial z & \partial f_z/\partial y \\ \partial f_y/\partial z & \partial f_y/\partial y \end{bmatrix} = \begin{bmatrix} -1-y & -z \\ (1+(\lambda-1))y/\varepsilon & ((\lambda-1)\,z-\varphi)/\varepsilon \end{bmatrix} \tag{16}$$

corresponding to the smallest eigenvalue with absolute value, at the origin $(z, y) = (0, 0)$, provides a good approximation of the slow invariant manifold only in a neighborhood of the

J. Stat. Mech. (2009) P06013

steady state (see, e.g., [14]). Hence, a set of points $\mathcal{G}_0$ along the straight line parallel to the latter eigenvector and passing through the steady state represents an initial approximation of the slow invariant manifold (squares in figure 1). Let $\boldsymbol{u} = [u_z, u_y]$ be the unit vector tangent to $\mathcal{G}_0$ at an arbitrary node. It proves convenient to define the following orthogonal projector matrix $\boldsymbol{P}$, for projection onto the tangent space $[u_z, u_y]$ of $\mathcal{G}$:

$$\boldsymbol{P} = \begin{bmatrix} u_z^2 & u_z u_y \\ u_y u_z & u_y^2 \end{bmatrix}. \tag{17}$$

In other words, the matrix $\boldsymbol{P}$ transforms an arbitrary vector into a new one parallel to $\boldsymbol{u}$. According to the MIG, a generic node (z^0, y^0) of the initial grid can be refined as follows:

$$z^1 = z^0 + \delta z, \qquad y^1 = y^0 + \delta y, \tag{18}$$

where the correction vector $[\delta z, \delta y]$ takes the explicit form

$$\begin{bmatrix} \delta z \\ \delta y \end{bmatrix} = \left(\boldsymbol{f}^{\mathrm{T}} - \boldsymbol{P}\boldsymbol{f}^{\mathrm{T}}\right) \delta t, \tag{19}$$

with $\boldsymbol{f} = [f_z, f_y]$, while δt is chosen of the order of a time step for integrating (15) using the explicit Euler scheme. However, estimates of δt can also be computed as suggested in [5]. MIG refinements are discussed in more detail in section 4.2. The collection of refined nodes forms the new grid $\mathcal{G}_1$, which can be further refined until the right-hand side of (19) becomes smaller than a fixed threshold. For instance, in figure 1 a refined grid (circles) is obtained after five iterations with $\delta t = 1 \times 10^{-2}$.

Remark. In the case of chemical reactive systems supported by thermodynamic Lyapunov functions (see section 2.2), the initial grid can be computed using the notion of a quasi-equilibrium manifold, as discussed in section 4.1. Moreover, a different construction of the projector matrix $\boldsymbol{P}$ is reviewed in section 4.2 (thermodynamic projector), which proves convenient in defining the fast directions in a general case (see, e.g., [7, 11]).

3.2. Grid based integrator

The slow dynamics of (15) obeys the following reduced equation:

$$\frac{\mathrm{d}\xi}{\mathrm{d}t} = \boldsymbol{l}\boldsymbol{P}\boldsymbol{f}^{\mathrm{T}}, \tag{20}$$

where $\xi = \boldsymbol{l}\boldsymbol{c}^{\mathrm{T}}$ is a parameter associated with the invariant grid node $\boldsymbol{c}$. Grid parameterization must be a unique mapping, and here we assume $\boldsymbol{l} = (1, 0)$. Notice that, though there are no general recipes for choosing the vector $\boldsymbol{l}$, some suggestions are presented in section 6.1 and [11, 12]. Starting from the initial condition ξ^0, (20) describes the slow dynamics of the full system (15) integrated from (z^0, y^0). More specifically, ξ^0 can be chosen as the grid parameter at the intersection point of the invariant grid and the straight line through (z^0, y^0) aligned with the fast directions. In our case, due to the smallness of the parameter ε in (15), fast motions occur along y; hence $\xi^0 = z^0$. Rigorous and more general definitions of fast and slow motions are provided in the literature on the basis of the notion of a thermodynamic projector [7, 11], and spectral decomposition of the Jacobian matrix [14]. The solution of (15) starting from $(z, y) = (0.75, 2)$, and the corresponding reduced solution of (20) are compared in figure 2. As a result, the reduced system recovers the asymptotic behavior with high accuracy once the fast dynamics gets exhausted.

J. Stat. Mech. (2009) P06013

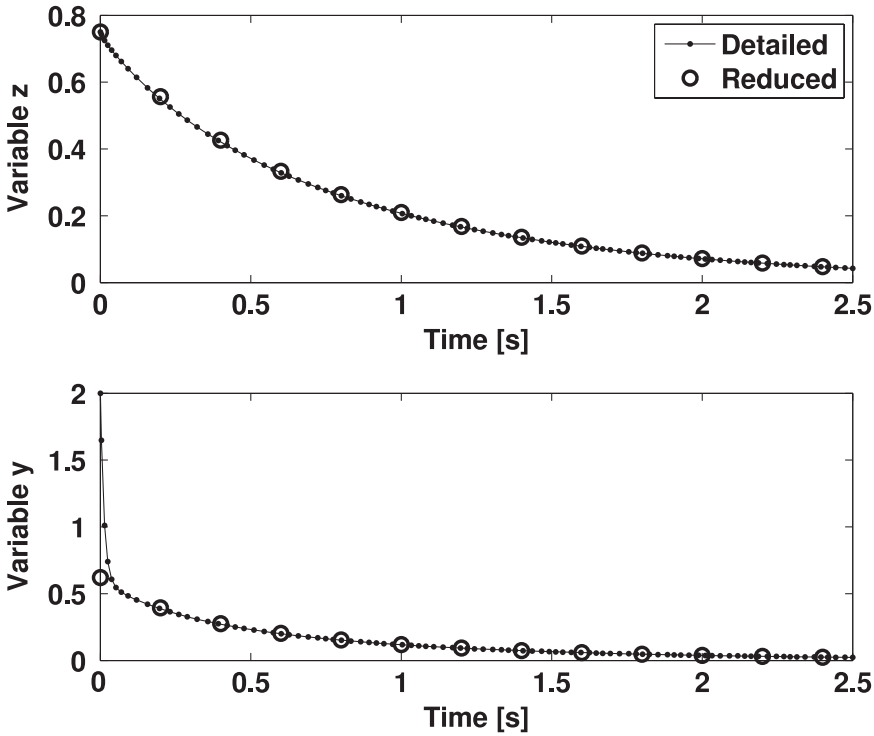

Figure 2. Comparison between detailed and reduced solutions. Initial condition: $(z, y) = (0.75, 2)$.

4. Model reduction technique

In our approach, we seek the reduced description of a batch reactor under the conditions described in section 2.1. The model reduction technique follows three steps:

(i) construction of the quasi-equilibrium grid using the algorithm introduced in [11],
(ii) refinement of the quasi-equilibrium grid via MIG iterations in order to get a better description of the SIM: the invariant grid,
(iii) invariant grid parameterization and construction of tables for lattice Boltzmann flow solvers.

These steps are briefly reviewed in the following sections.

4.1. Quasi-equilibrium grid

By definition, a q-dimensional QEM is a manifold in the space of concentration which minimizes the Lyapunov function (10) under a set of q linear constraints. Let us consider the minimization problem

$$\min\ G \qquad \text{s.t.}\ \sum_{i=1}^{n} l_i^j Y_i = \xi^j, \qquad j = 1, \ldots, q, \tag{21}$$

where $\{\boldsymbol{l}^j = (l_1^j, \ldots, l_n^j)\}$ is a set of q fixed vectors and their choice will be discussed in section 6.1. Because of the convexity of G, once q values are assigned to the quantities

ξ^j, the solution of (21) is unique when it exists. For a detailed discussion about the mathematical properties of (21), the interested reader is referred to [3, 4]. Regarding ξ^j as variables, the full set of constrained minima forms the q-dimensional quasi-equilibrium manifold (QEM) corresponding to the vector set $\{\boldsymbol{l}^j\}$.

As suggested in [4, 5], the QEM provides a reasonably good initial approximation of the slow invariant manifold (SIM). Comparisons between QEM and SIM can be found in [6, 11] for a range of problems.

Before proceeding further, we note that the QEM can be of interest for model reduction even before any of its refinement is addressed. For instance, the rate-controlled constrained-equilibrium (RCCE) method uses directly the notion of the QEM for simplifying reaction mechanisms in combustion [8]–[10].

For the sake of completeness, below we briefly review the quasi-equilibrium grid algorithm [11] for constructing a discrete analog of a QEM. Let $\boldsymbol{D}$ be the $d \times n$ matrix whose (i,k)-element is μ_{ik}/W_i. Let $\boldsymbol{E}$ be the $(d+q) \times n$ matrix, constructed by adding the $\boldsymbol{l}^j$ vectors as q additional rows to $\boldsymbol{D}$. Assume that the steady state of (5) is $\boldsymbol{\psi}^0 = (p, \bar{h}, Y_1^0, \ldots, Y_n^0)$ while the gradient and the second-derivative matrix of G are

$$\boldsymbol{\nabla} G = \left(\frac{\partial G}{\partial Y_i}\right)_{p,\bar{h}}, \qquad \boldsymbol{H} = \left[\frac{\partial^2 G}{\partial Y_i \partial Y_j}\right]_{p,\bar{h}}, \tag{22}$$

where all the derivatives are computed for fixed pressure and mixture-averaged enthalpy. A QEM state $\boldsymbol{\psi}^1$ can be computed, in a neighborhood of $\boldsymbol{\psi}^0$, by solving the linear algebraic system

$$\begin{aligned}
&\sum_{i=1}^{z} \left(\boldsymbol{t}_j \boldsymbol{H} \boldsymbol{\rho}_i^{\mathrm{T}}\right) \varphi_i = -\boldsymbol{\nabla} G \boldsymbol{t}_j^{\mathrm{T}} \quad j = 1, \ldots, z-q,\\
&\sum_{i=1}^{z} \left(\boldsymbol{l}^1 \boldsymbol{\rho}_i^{\mathrm{T}}\right) \varphi_i = 0,\\
&\vdots\\
&\sum_{i=1}^{z} \left(\boldsymbol{l}^k \boldsymbol{\rho}_i^{\mathrm{T}}\right) \varphi_i = \varepsilon_k,\\
&\vdots\\
&\sum_{i=1}^{z} \left(\boldsymbol{l}^q \boldsymbol{\rho}_i^{\mathrm{T}}\right) \varphi_i = 0.
\end{aligned} \tag{23}$$

If $\{\boldsymbol{\rho}_1, \ldots, \boldsymbol{\rho}_z\}$ and $\{\boldsymbol{t}_1, \ldots, \boldsymbol{t}_{z-q}\}$ are two vector bases in the null space of matrix $\boldsymbol{D}$ and $\boldsymbol{E}$, respectively, then

$$\boldsymbol{\psi}^1 = \left(p, \bar{h}, Y_1^0 + \mathrm{d}Y_1, \ldots, Y_n^0 + \mathrm{d}Y_n\right), \qquad (\mathrm{d}Y_1, \ldots, \mathrm{d}Y_n) = \sum_{i=1}^{z} \varphi_i \boldsymbol{\rho}_i. \tag{24}$$

Referring to system (23), all derivatives of G are evaluated at $\boldsymbol{\psi}^0$ and, through the last q equations, we impose that $\boldsymbol{\psi}^1$ belongs to a Cartesian grid in the space $\{\xi^1, \ldots, \xi^q\}$, with the fixed parameter ε_k defining the grid step along ξ^k. Similarly, by solving (23) at $\boldsymbol{\psi}^1$, a

J. Stat. Mech. (2009) P06013

new QEM point $\boldsymbol{\psi}^2$ can be found. In general, this procedure can be iterated as long as all the coordinates of the computed state are non-negative. The collection of computed states is called the *quasi-equilibrium grid*.

4.2. Refinement procedure

Assuming that the slow dynamics of (5) approximately evolves along a QEM, the corresponding quasi-equilibrium grid might be directly used for the reduced description of the detailed system. However, the QEM (and its discrete form) generally provides only an approximation of the slow invariant manifold [5], [10]–[12], and the method of invariant grids (MIG) enables us to refine it. A brief discussion on the MIG implementation is in order (see also the *relaxation methods* in [5, 7]).

Assume that, at any QEM point, the tangent plane τ is defined and spanned by q vectors

$$\boldsymbol{u}_i = \partial \boldsymbol{F}/\partial \xi^i, \quad i = 1, \ldots, q, \tag{25}$$

where a smooth function $\boldsymbol{F}(\xi_1, \ldots, \xi_q)$, mapping the variables $\{\xi^1, \ldots, \xi^q\}$ into the state space $\{Y_1, \ldots, Y_n\}$, is a solution to the problem (21). Typically, the tangent vectors can be defined at a point of a quasi-equilibrium grid by approximating (25) via finite differences. Let $\boldsymbol{P}$ be any $(n \times n)$ matrix (projector), defined at the quasi-equilibrium grid point $\boldsymbol{\psi}$, such that the image $\mathrm{im}(\boldsymbol{P}) \equiv \tau$ and $\boldsymbol{P}^2 = \boldsymbol{P}$. In general, if the vector field $\boldsymbol{f} = (\mathrm{d}Y_1/\mathrm{d}t, \ldots, \mathrm{d}Y_n/\mathrm{d}t)^{\mathrm{T}}$ is computed at $\boldsymbol{\psi}$, the *invariance defect*

$$\boldsymbol{\Delta}(\boldsymbol{\psi}) = \boldsymbol{f} - \boldsymbol{P}\boldsymbol{f} \tag{26}$$

does not vanish, whereas it does so in the case of an invariant manifold. According to the MIG, any state of the initial grid $\boldsymbol{\psi} = (p, \bar{h}, Y_1, \ldots, Y_n)$ can be corrected and replaced by $\boldsymbol{\psi}^*$ where

$$\boldsymbol{\psi}^* = \left(p, \bar{h}, Y_1 + \mathrm{d}Y_1, \ldots, Y_n + \mathrm{d}Y_n\right), \qquad (\mathrm{d}Y_1, \ldots, \mathrm{d}Y_n) = \delta t \boldsymbol{\Delta}(\boldsymbol{\psi}). \tag{27}$$

The collection of states $\boldsymbol{\psi}^*$ forms a new grid, where the matrix $\boldsymbol{P}$ can be updated and the corrections (27) applied again. The parameter δt has the dimension of time and it is chosen of the order of magnitude of the time step needed for integrating (5) using the explicit Euler scheme. This iterative procedure ends when, at any grid point, the Euclidean norm of the invariance defect, compared to the norm of the vector field $\boldsymbol{f}$, is smaller than a fixed threshold. The last set of states is called the invariant grid.

Moreover, we recommend a special construction of $\boldsymbol{P}$ reported below at a given point $\boldsymbol{\psi}$. Let $\ker(\boldsymbol{\nabla} G)$ be the plane orthogonal to $\boldsymbol{\nabla} G$ and $\tau_0 = \tau \cap \ker(\boldsymbol{\nabla} G)$, with $\tau \neq \tau_0$. Let the vector $\hat{\boldsymbol{u}}_1$ of τ fulfil the conditions

$$\boldsymbol{\nabla} G \hat{\boldsymbol{u}}_1^{\mathrm{T}} = 1, \quad \hat{\boldsymbol{u}}_1 \boldsymbol{H} \boldsymbol{\eta}^{\mathrm{T}} = 0, \qquad \forall \boldsymbol{\eta} \in \tau_0. \tag{28}$$

Assume that $\{\hat{\boldsymbol{u}}_2, \ldots, \hat{\boldsymbol{u}}_n\}$ is a vector basis of τ_0 such that $\hat{\boldsymbol{u}}_i \boldsymbol{H} \hat{\boldsymbol{u}}_j^{\mathrm{T}} = \delta_{ij}$, where δ_{ij} denotes the Kronecker delta. In the case $\tau \equiv \tau_0$, let $\{\hat{\boldsymbol{u}}_1, \ldots, \hat{\boldsymbol{u}}_n\}$ be a vector basis of τ such that $\hat{\boldsymbol{u}}_i \boldsymbol{H} \hat{\boldsymbol{u}}_j^{\mathrm{T}} = \delta_{ij}$. $\boldsymbol{P}$ is called a *thermodynamic projector* if it is constructed as follows:

$$\boldsymbol{P} = \boldsymbol{P}_1 + \sum_{k=2}^{n} \boldsymbol{P}_k, \qquad \boldsymbol{P}_1(i,j) = \boldsymbol{\nabla} G_j \hat{\boldsymbol{u}}_{1i}, \qquad \boldsymbol{P}_k(i,j) = (\hat{\boldsymbol{u}}_k \boldsymbol{H})_j \hat{\boldsymbol{u}}_{ki}. \tag{29}$$

4.3. Grid tabulation

The slow dynamics of (5) takes place along the invariant grid and obeys the reduced q-dimensional system

$$\frac{\mathrm{d}\xi^i}{\mathrm{d}t} = \boldsymbol{l}^i \boldsymbol{P} \boldsymbol{f}^{\mathrm{T}}, \qquad i = 1, \ldots, q. \tag{30}$$

Once the invariant grid is obtained, it can be stored in tables for later use in the flow solver. The grid parameterization is performed by attaching, to any grid state, the q quantities ξ^j, evaluated according to (21). The coordinates at every grid point, the corresponding temperature, the right-hand side of (30) and each component of the projected vector field $\boldsymbol{P}\boldsymbol{f}^{\mathrm{T}}$ are collected in q-dimensional arrays and can be accessed through the grid parameters ξ^j.

Remark. On the invariant grid, the thermodynamic projector performs fast–slow motion decomposition of the vector field $\boldsymbol{f}$. In other words, the fast component of $\boldsymbol{f}$ belongs to the null space of the matrix (29) (see [7]). For this reason, the projector in (30) must be thermodynamic, whereas for the refinement procedure (27) we may use a different projector matrix.

5. Lattice Boltzmann method for reactive flows

We consider here the simplest lattice Boltzmann formulation suitable for simulations of combustion. To this end, following the suggestion of Yamamoto *et al* [19], reactive flows can be simulated with the lattice Boltzmann (LB) method as reported in section 5.1.

Note, however, that more elaborate and complete LB models for mixtures [16, 17] and compressible flows [18] will be taken into account in the near future, too.

5.1. Original model

Let us consider the 1D three-bit lattice (figure 3). We assume that the flow field is not affected by the chemical reaction, transport coefficients are constant and Fick's law applies to the diffusion. The evolution equation of pressure populations, for the incompressible model, is

$$p_\alpha\left(x + e_\alpha, t + \Delta t\right) = p_\alpha\left(x, t\right) - \frac{1}{\tau_{\mathrm{F}}}\left[p_\alpha\left(x, t\right) - p_\alpha^{\mathrm{eq}}\left(p, v\right)\right], \tag{31}$$

where the equilibrium populations take the form

$$p_\alpha^{\mathrm{eq}}\left(p, v\right) = w_\alpha p\left[1 + 3\left(e_\alpha v\right) + \tfrac{9}{2}\left(e_\alpha v\right)^2 - \tfrac{3}{2}v^2\right], \tag{32}$$

with $w_0 = 1/3$, $w_+ = w_- = 1/6$. The total pressure p and the fluid velocity v read

$$p = \sum_\alpha p_\alpha, \qquad v = \frac{1}{p_0}\sum_\alpha e_\alpha p_\alpha. \tag{33}$$

J. Stat. Mech. (2009) P06013

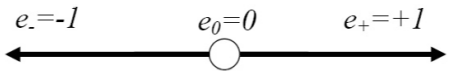

Figure 3. D1Q3 stencil. Three discrete velocities on a 1D lattice.

The reference pressure is $p_0 = \rho_0/3$, ρ_0 being the constant density of the model in LB units. Let Δt be the time step; the relaxation parameter τ_{F} is related to the kinematic viscosity ν by

$$\nu = \frac{2\tau_{\mathrm{F}} - 1}{6}\Delta t. \tag{34}$$

Let T_0 be a reference temperature; the evolution equations for the temperature and concentration of species i are written as

$$\begin{aligned} \tilde{T}_\alpha\left(x + e_\alpha, t + \Delta t\right) - \tilde{T}_\alpha\left(x, t\right) &= -\frac{1}{\tau_T}\left[\tilde{T}_\alpha\left(x, t\right) - \tilde{T}_\alpha^{\mathrm{eq}}\left(\tilde{T}, v\right)\right] + w_\alpha Q_T, \\ Y_{i\alpha}\left(x + e_\alpha, t + \Delta t\right) - Y_{i\alpha}\left(x, t\right) &= -\frac{1}{\tau_{Y_i}}\left[Y_{i\alpha}\left(x, t\right) - Y_{i\alpha}^{\mathrm{eq}}\left(Y_i, v\right)\right] + w_\alpha Q_{Y_i}, \end{aligned} \tag{35}$$

where

$$\tilde{T} = T/T_0 = \sum_\alpha T_\alpha, \qquad Y_i = \sum_\alpha Y_{i\alpha}, \tag{36}$$

and the equilibrium populations $\tilde{T}_\alpha^{\mathrm{eq}}$, $Y_{i\alpha}^{\mathrm{eq}}$ are expressed as in (32) after replacing p with $\tilde{T}$ and Y_i, respectively. Assume that t_0 is a factor for converting physical time into LB time units: $(t)_{\mathrm{LB}} = (t)_{\mathrm{phys}}/t_0$. The source terms take the explicit form

$$Q_T = \frac{1}{T_0}\left(\sum_{i=1}^{n}\frac{\dot{\omega}_i W_i}{\bar{\rho}c_p}h_i\right)t_0\Delta t, Q_{Y_i} = \frac{\dot{\omega}_i W_i}{\bar{\rho}}t_0\Delta t, \tag{37}$$

where c_p is the mean specific heat of the mixture per unit mass at constant pressure. The thermal diffusivity κ and diffusion coefficient D_i of species i are related to the relaxation parameters as follows:

$$\kappa = \frac{2\tau_T - 1}{6}\Delta t, \qquad D_i = \frac{2\tau_{Y_i} - 1}{6}\Delta t. \tag{38}$$

5.2. Hydrodynamic limit

In section 5.1, we briefly review the lattice Boltzmann model for reactive flows originally presented in [19], where more details can be found. However, it is worth reporting here the basic assumptions of the model:

- There are no external forces.
- The chemical reaction does not affect the flow field in an incompressible model.
- The transport properties are constant.
- The diffusion follows Fick's law.
- Viscous energy dissipation and radiative heat loss are neglected.

J. Stat. Mech. (2009) P06013

A detailed discussion on fundamental aspects of the lattice Boltzmann equation (31), derivation of the equilibrium populations (32), relations between transport coefficients and relaxation parameters (e.g. (34) and (38)) can be found in [20]. According to [19], the lattice Boltzmann equations (35) simulate, in the hydrodynamic limit, the following partial differential equations (PDE) written for one-dimensional problems:

$$\frac{\partial T}{\partial t} + v\frac{\partial T}{\partial x} = \kappa\frac{\partial^2 T}{\partial x^2} + \sum_{i=1}^{n}\frac{\dot{\omega}_i W_i}{\bar{\rho}c_p}h_i, \tag{39}$$

and

$$\bar{\rho}\left(\frac{\partial Y_i}{\partial t} + v\frac{\partial Y_i}{\partial x}\right) = D_i\frac{\partial}{\partial x}\left(\bar{\rho}\frac{\partial Y_i}{\partial x}\right) + \dot{\omega}_i W_i, \tag{40}$$

which account for the conservation of energy and a generic species x_i, respectively. It is worth stressing here that the PDE (39) is valid under the assumption of constant mean specific heat c_p. More generally, conservation of energy can be written in terms of the mixture-averaged enthalpy $\bar{h}$ as follows:

$$\frac{\partial \bar{h}}{\partial t} + v\frac{\partial \bar{h}}{\partial x} = \kappa\frac{\partial^2 \bar{h}}{\partial x^2} + \sum_{i=1}^{n}\frac{\dot{\omega}_i W_i}{\bar{\rho}}h_i, \tag{41}$$

while (39) is recovered neglecting the dependence of c_p on temperature, and recording that $\bar{h} = c_p T$. As a result, the first equation in (35) can be also expressed in terms of populations representing the mixture-averaged enthalpy:

$$\tilde{h}_\alpha\left(x + e_\alpha, t + \Delta t\right) - \tilde{h}_\alpha\left(x, t\right) = -\frac{1}{\tau_T}\left[\tilde{h}_\alpha\left(x, t\right) - \tilde{h}_\alpha^{\mathrm{eq}}\right] + w_\alpha Q_h. \tag{42}$$

Here, we have reformulated the temperature evolution equations in terms of dimensionless enthalpy: $\tilde{h} = h/h_0$, with h_0 a reference enthalpy. Now, the equilibrium populations and the heat source term are given by

$$\begin{aligned}\tilde{h}_\alpha^{\mathrm{eq}} &= w_\alpha\tilde{h}\left[1 + 3\left(e_\alpha v\right) + \tfrac{9}{2}\left(e_\alpha v\right)^2 - \tfrac{3}{2}v^2\right],\\ Q_h &= \frac{1}{h_0}\left(\sum_{i=1}^{n}\frac{\dot{\omega}_i W_i}{\bar{\rho}}h_i\right)t_0\Delta t.\end{aligned} \tag{43}$$

In the following, the energy conservation equation will be used in the form (42), because the mixture-averaged enthalpy is an explicit parameter of the reduced model construction, as illustrated later on in section 6.1.

5.3. Modified algorithm

The slow manifold, constructed by the procedure of section 4, is invariant under the dynamics of system (5), which only accounts for the chemical source term. Since, at any lattice point of the domain, the LB equations also contain advection and diffusion terms, the computed grid is not invariant with respect to the LB dynamics (see figure 4). On the other hand, the time scales associated with chemical reactions are typically faster than the time scales of the flow. In this case, we can still use the chemical slow invariant manifold for speeding up computations. To this end, we suggest the following modifications to the

J. Stat. Mech. (2009) P06013

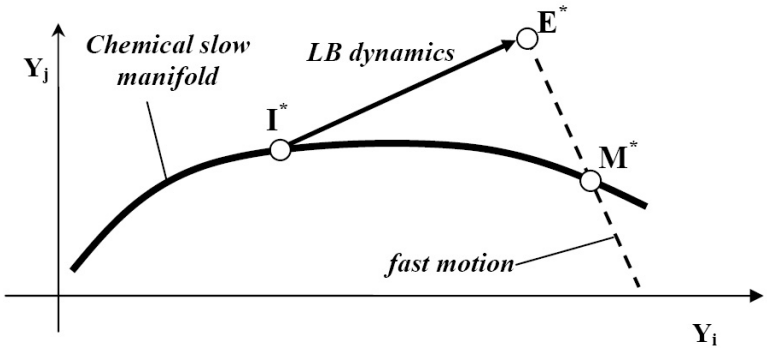

Figure 4. Starting from an initial state I^*, the LB dynamics runs out of the chemical slow manifold.

LB algorithm of section 5.1, where the energy equation is written according to (42):

- COLLISION:

$$\begin{aligned} \tilde{h}^*_\alpha(x,t) &= \tilde{h}_\alpha(x,t) - \frac{1}{\tau_T}\left[\tilde{h}_\alpha(x,t) - \tilde{h}^{\mathrm{eq}}_\alpha(h,v)\right], \\ \tilde{Y}_{i\alpha}(x,t) &= Y_{i\alpha}(x,t) - \frac{1}{\tau_{Y_i}}\left[Y_{i\alpha}(x,t) - Y^{\mathrm{eq}}_{i\alpha}(Y,v)\right], \end{aligned} \tag{44}$$

- STREAMING + REACTION:

$$\begin{aligned} \tilde{h}_\alpha(x+e_\alpha, t+\Delta t) &= \tilde{h}^*_\alpha(x,t) + w_\alpha Q_h, \\ \tilde{Y}^*_{i\alpha}(x+e_\alpha, t+\Delta t) &= \tilde{Y}_{i\alpha}(x,t) + w_\alpha Q_{Y_i}, \end{aligned} \tag{45}$$

- POPULATION CORRECTION:

$$Y_{i\alpha}(x,t) = Y^*_{i\alpha}(x,t) + \psi_{i\alpha}. \tag{46}$$

The correction step (46) can be understood by referring to figure 4. The LB dynamics brings the initial state I^* (located on the chemical slow manifold) to the point E^* (off-manifold). Nevertheless, assuming that such a manifold is still attractive for the overall dynamics, E^* has to quickly relax to the point M^*. This relaxation occurs along the local fast direction, towards a manifold computed under the fixed mixture enthalpy and element fractions (12) of state E^*. Let $(M^* - E^*)(i)$ be the ith element of vector $(M^* - E^*)$. The correction terms are evaluated using the conditions

$$\sum_\alpha \psi_{i\alpha} = (M^* - E^*)(i), \qquad \sum_\alpha e_\alpha \psi_{i\alpha} = 0, \qquad \sum_\alpha e_\alpha^2 \psi_{i\alpha} = 0, \tag{47}$$

meaning that the zeroth-order moment of $Y_{i\alpha}$ collapses from E^* to M^*, while none of the other moments are affected. The conditions (47) are written for the 1D lattice of figure 3, but the same idea can be applied to any lattice.

The procedure described is intended to get rid of the fast motions which require explicit solvers, such as the LB method, to choose a small time step. Finally, notice that the source terms in (45) are now obtained from tables via interpolation.

J. Stat. Mech. (2009) P06013

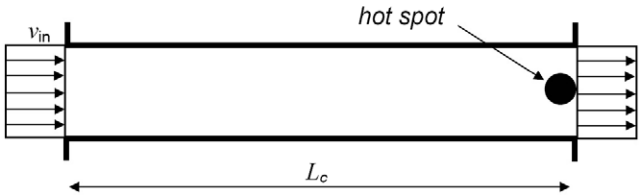

Figure 5. Schematic representation of the 1D setup.

6. Example: plane flame propagation

In the following, we consider a stoichiometric hydrogen–air mixture entering an adiabatic channel (constant cross section) under room conditions ($T = 300$ K, $p = 1$ bar) at fixed velocity. A heat source is placed at the outlet in order to ignite the mixture (see figure 5). The background flow, from equation (31), keeps both pressure and velocity fields uniform in space and time. A flame front is formed and propagates upstream since the laminar flame speed is larger than the flow velocity. For simplicity, we use the assumption of equal diffusivity D for all species and Lewis number $Le = \kappa/D = 1$. In this case, the mixture enthalpy $\bar{h}$ and the element fractions (12) remain constant throughout the domain, and the reduced dynamics takes place along the invariant grid constructed as illustrated in section 4. Notice that the latter assumption is not restricting and a generalization is obtained by extending the invariant grid with enthalpy and element fractions as additional degrees of freedom. On the other hand, in premixed systems, those quantities are conserved up to small fluctuations and, for such applications, the invariant grid is often sufficient. Finally, in combustion, the pressure p can be considered constant for most cases.

6.1. 2D reduced description

In our study, the detailed mechanism of Li *et al* [13] (9 species, 21 elementary reactions) for hydrogen combustion is considered, and we search for a reduced description with only two degrees of freedom. To this end, let us construct the 2D quasi-equilibrium grid for a stoichiometric H_2–air mixture under fixed pressure $p = 1$ bar and enthalpy $\bar{h} = 2.8$ kJ kg^{-1}, corresponding to the temperature $T_0 = 300$ K for the unburned mixture $H_2 + 0.5O_2 + 1.88N_2$. The vector set $\{\boldsymbol{l}^j\}$ in (21) is used to reparameterize the original variables Y_i in terms of new ones ξ^j, which are expected to follow a slow dynamics. Many suggestions for defining slow lumped variables in chemical kinetics are known in the literature, and for our purposes we use

$$\xi^1 = \sum_{i=1}^{9} \frac{Y_i}{W_i}, \qquad \xi^2 = \frac{Y_{\mathrm{O}}}{W_{\mathrm{O}}} + \frac{Y_{\mathrm{OH}}}{W_{\mathrm{OH}}} + \frac{Y_{\mathrm{H_2O}}}{W_{\mathrm{H_2O}}}, \tag{48}$$

expressing the *total number of moles* (slow dissociation/recombination reactions) and *free oxygen* (slow reactions where the O–O bond is broken), respectively (see, e.g., [10]). A different choice of the reduced variables, based on the Jacobian matrix of system (5) at the steady state, can also be found in [6]. It is important to stress that, though the choice of $\{\boldsymbol{l}^j\}$ affects the accuracy of the quasi-equilibrium grid in describing the slow manifold,

J. Stat. Mech. (2009) P06013

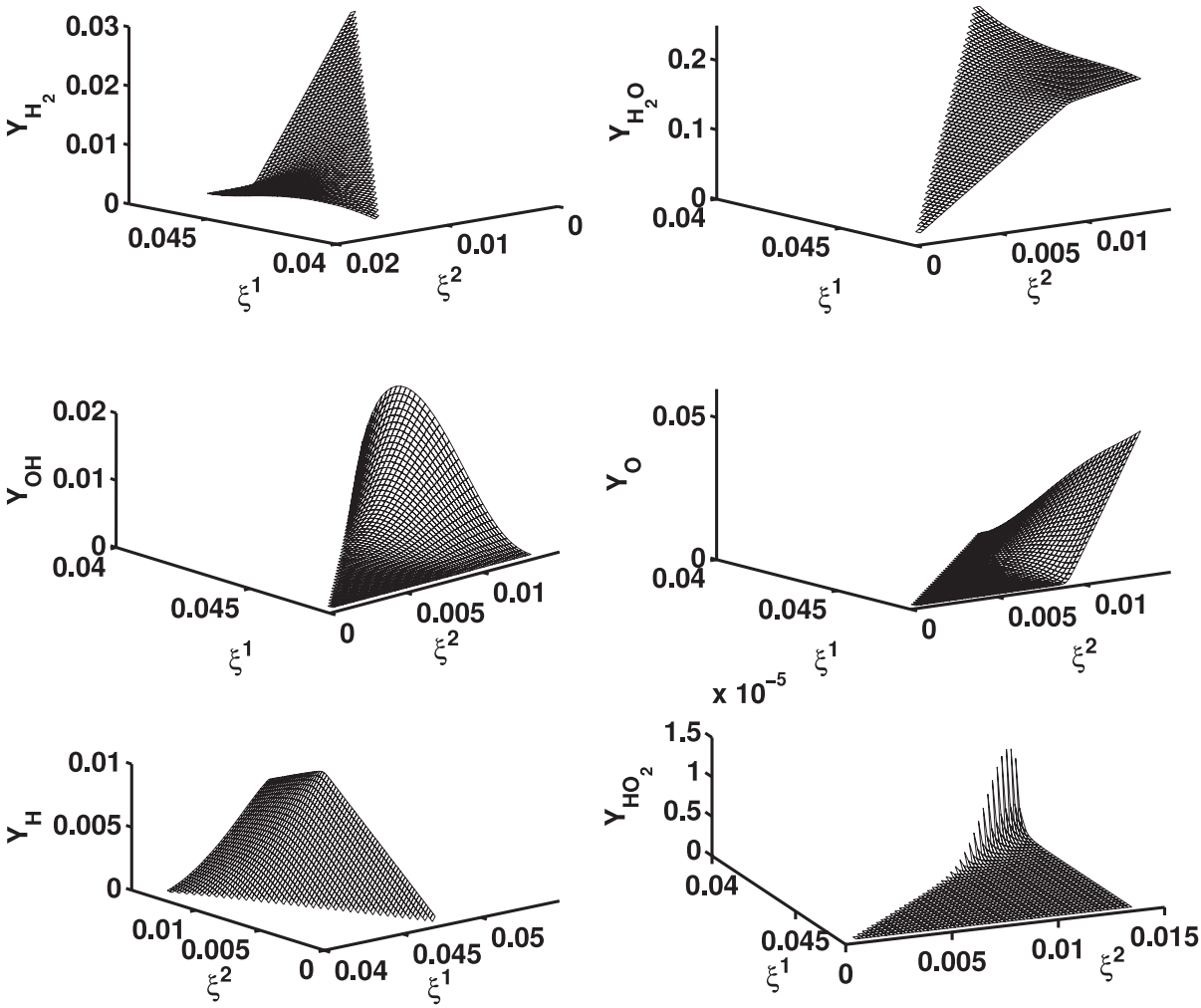

Figure 6. Six coordinates of the 2D quasi-equilibrium grid for a stoichiometric H_2–air mixture, under $p = 1$ bar and $\bar{h} = 2.8$ kJ kg^{-1}.

that grid is anyway refined (see section 4.2) and the final result does not depend on the initial grid. First of all, starting from the steady state, equations (23) are solved moving along ξ^1 with $\varepsilon_1 = 1.8 \times 10^{-4}$; second the grid grows along ξ^2 with $\varepsilon_2 = \varepsilon_1$ and the construction ends when the concentration point, corresponding to the unburned mixture, is reached. The 2D quasi-equilibrium grid, shown in figure 6, is relaxed to the invariant grid using equation (27), where the projector is thermodynamic and constructed as illustrated in (29). We have chosen the parameter $\delta t = 1 \times 10^{-8}$ and the convergence ratio between the invariance defect and the vector field was set at $|\boldsymbol{\Delta}|/|\boldsymbol{f}| \leq 0.01$ at any grid node. Whenever that ratio keeps increasing while refining, the corresponding grid node is discarded. The 2D refined grid is shown in figure 7, and it is compared to the initial quasi-equilibrium grid in figure 8. Notice that in the low temperature region ($T < 800$ K), the invariant grid is not convergent, meaning that a 2D description is not enough and the dimension of the slow invariant manifold is larger than 2. The grid coordinates, the thermodynamic projection of the vector field $\boldsymbol{f}$ and the two parameters

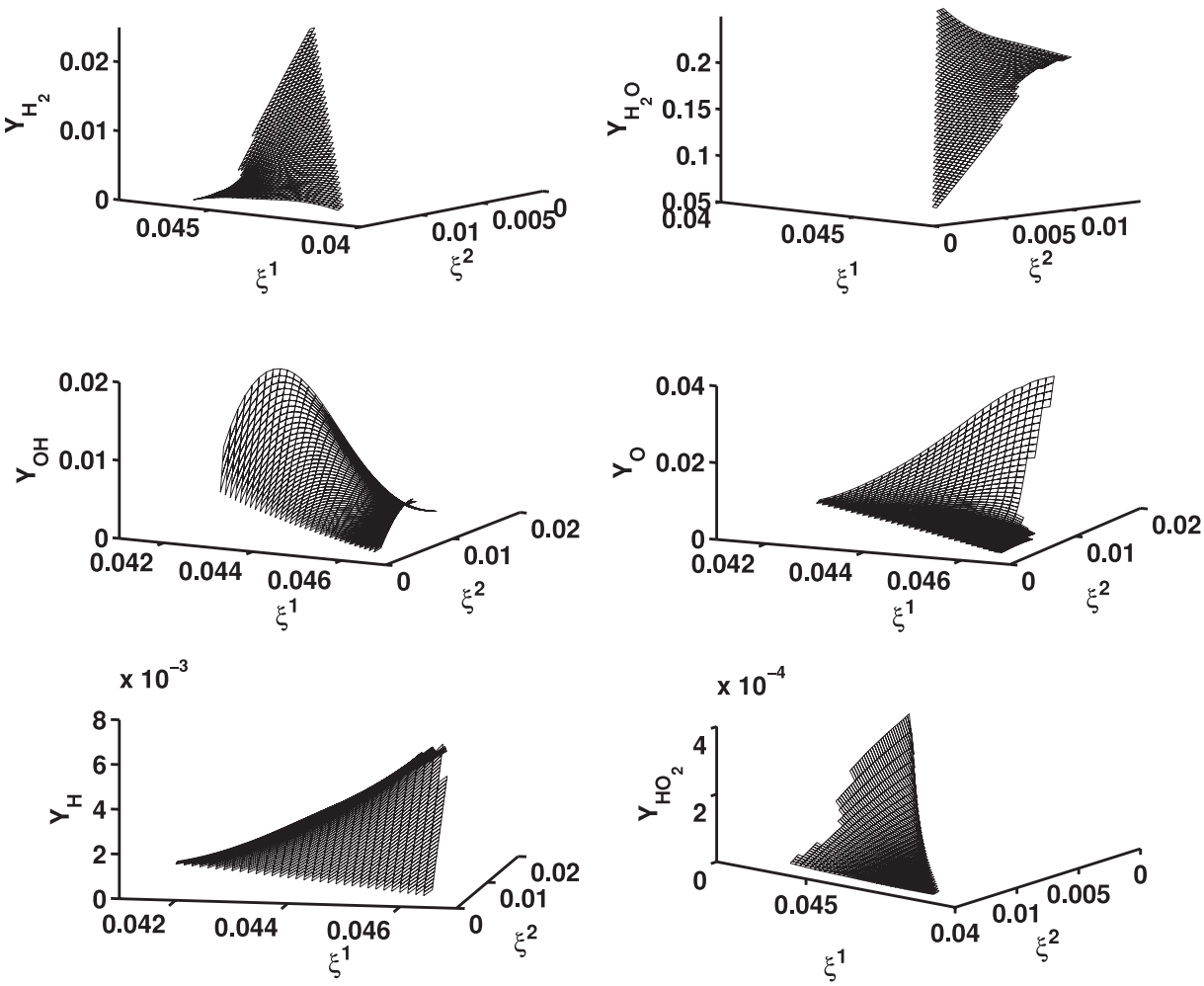

Figure 7. Six coordinates of the refined 2D invariant grid for a stoichiometric H_2–air mixture, under $p = 1$ bar and $\bar{h} = 2.8$ kJ kg^{-1}.

ξ_1, ξ_2 are stored in two-dimensional arrays and each grid node is identified by an index pair (i, j). Any tabulated quantity $\tilde{Q}$, associated with a generic parameter pair (ξ^1, ξ^2), is reconstructed by linear bi-variate interpolation:

$$\tilde{Q} = \iota_A \tilde{Q}_A + \iota_B \tilde{Q}_B + \iota_C \tilde{Q}_C + \iota_D \tilde{Q}_D, \tag{49}$$

where A, B, C, D are the grid nodes corresponding to (i, j), $(i{+}1, j)$, $(i, j{+}1)$, $(i{+}1, j{+}1)$, respectively, while ι_A, ι_B, ι_C, ι_D are the Lagrangian weights

$$\begin{aligned} \iota_A &= (1 - \pi_1)(1 - \pi_2), \qquad \iota_B = \pi_1 (1 - \pi_2), \\ \iota_C &= (1 - \pi_1)\pi_2, \qquad \iota_D = \pi_1 \pi_2, \end{aligned} \tag{50}$$

with $\pi_1 = (\xi^1 - \xi^1_A)/(\xi^1_B - \xi^1_A)$ and $\pi_2 = (\xi^2 - \xi^2_A)/(\xi^2_C - \xi^2_A)$.

6.2. Setup and comparisons

In the simulation, the length of the adiabatic channel is $L_c = 5$ mm, the inlet velocity $v_{in} = 1.2$ m s^{-1} and the species diffusivity $D = 5 \times 10^{-5}$ m^2 s^{-1}. All quantities given in

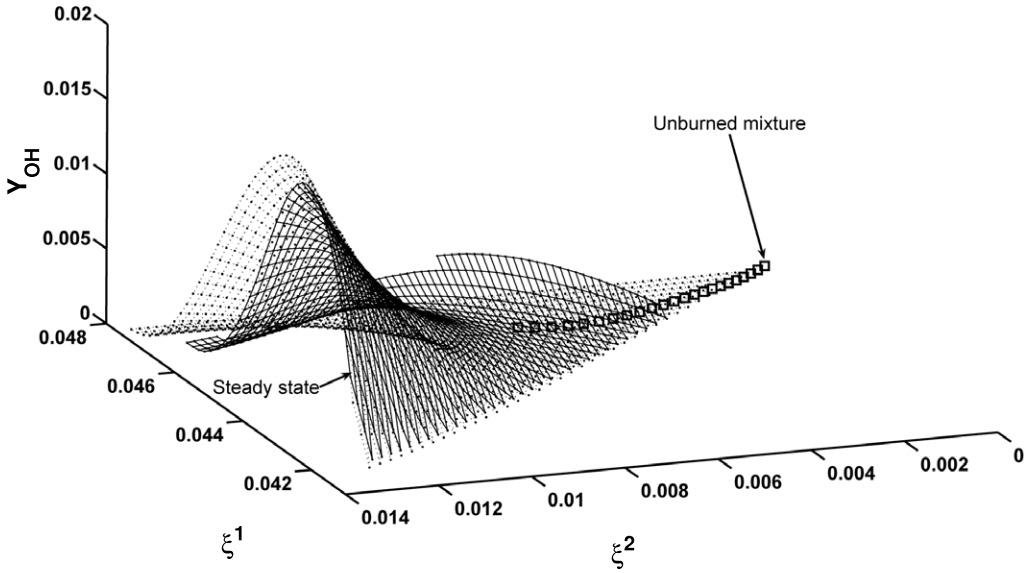

Figure 8. OH coordinate: 2D quasi-equilibrium grid (dashed lines), 2D invariant grid (continuous lines), trajectory starting from the unburned mixture (squares).

physical units of time (s) and length (m) are converted into LB units, dividing by the factors

$$t_0 = \frac{(L_c/v_{in})_{phys}}{(L_c/v_{in})_{LB}}, \qquad L_0 = \frac{(L_c)_{phys}}{(L_c)_{LB}}, \tag{51}$$

respectively. Let Δx be the space step, the time step

$$\Delta t_{LB} = \left(\frac{\Delta x}{e}\right)_{LB}, \qquad \Delta t_{phys} = t_0 \Delta t_{LB} \tag{52}$$

is set by defining the ratio $(L_c/v_{in})_{LB}$, and e is the magnitude of the non-zero lattice velocities of figure 3. The initial profiles are flat, corresponding to the unburned mixture with $T = 300$ K, everywhere except in a neighborhood of the outlet, where the temperature peaks up to $T = 1400$ K, in order to let the mixture ignite. At the inlet, the initial conditions are imposed while, at the outlet, the fully developed boundary conditions are used for every field. Because of the stiffness of the chemical source term, a stable computation, carried out by using the model in section 5.1, requires $\Delta t_{phys} \leq 6 \times 10^{-8}$ s. Notice that, due to the unity Lewis number, the enthalpy is uniform in space and the temperature is given by solving the first equation in (6). An identical setup can also be simulated using the modified algorithm of section 5.3, where the reduced description is provided either by the 2D quasi-equilibrium grid or by the refined invariant grid. The latter option is chosen; the result is shown in figure 9 and compared to the solution of the original detailed reaction model. The invariant grid does not extend into the low temperature zone: here, the source terms are evaluated as in the original model and the correction step (46) is not performed. For simplicity, on the basis of the assumption that the variables (48) are slow over the whole concentration space, the point M^* of figure 4 is the grid state which corresponds to the pair (ξ^1, ξ^2) computed at E^*. The agreement

J. Stat. Mech. (2009) P06013

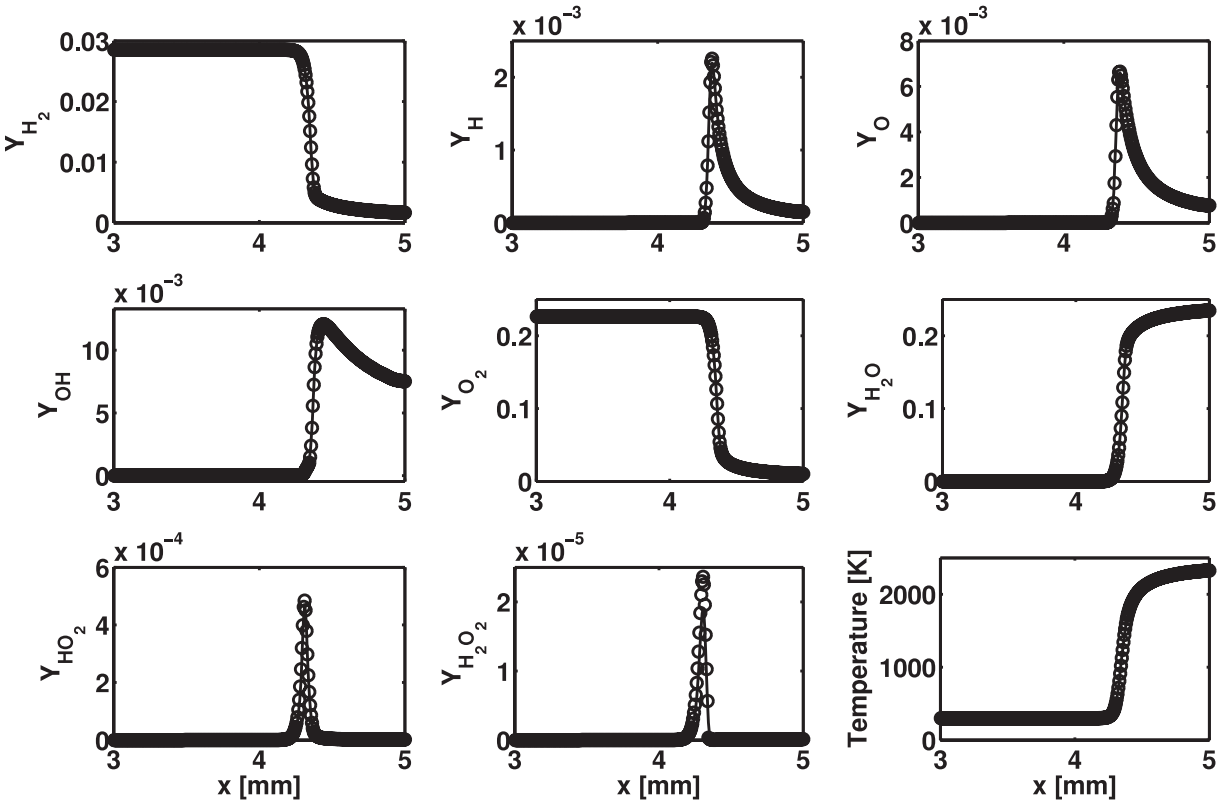

Figure 9. Fields along the channel at a given time: detailed model (continuous line) and reduced model (circles).

between the two models is excellent and, using the modified algorithm, computations are stable with the time step $\Delta t_{\text{phys}} \leq 5 \times 10^{-7}$ s. Moreover, in the latter case the extra effort, due to an additional step (46), is counterbalanced by savings during the computation of the chemical source terms: those quantities do indeed demand the evaluation of exponential functions (see (2) and (3)), whereas for the reduced model a fast look-up table is adopted. As a result, in our simulations, the modified sequence of section 5.3, with interpolated source terms Q_{Y_i}, is about 30% faster than the detailed reaction algorithm, where the Q_{Y_i} are explicitly computed. Overall, the suggested methodology exhibits a speedup of ten times.

6.3. Dimension reduction

Let all species have equal diffusivity D; a projection of the species evolution equations in (35) onto the invariant grid, according to the slow variables (48), gives

$$\begin{aligned} \tilde{h}_\alpha\left(x+e_\alpha, t+1\right) - \tilde{h}_\alpha\left(x,t\right) &= -\frac{1}{\tau_T}\left[\tilde{h}_\alpha\left(x,t\right) - \tilde{h}_\alpha^{\text{eq}}\left(h,v\right)\right] + w_\alpha Q_h, \\ \xi_\alpha^j\left(x+e_\alpha, t+1\right) - \xi_\alpha^j\left(x,t\right) &= -\frac{1}{\tau_\xi}\left[\xi_\alpha^j(x,t) - \xi_\alpha^{j\text{eq}}\left(\xi^j, v\right)\right] + w_\alpha Q_{\xi^j}. \end{aligned} \tag{53}$$

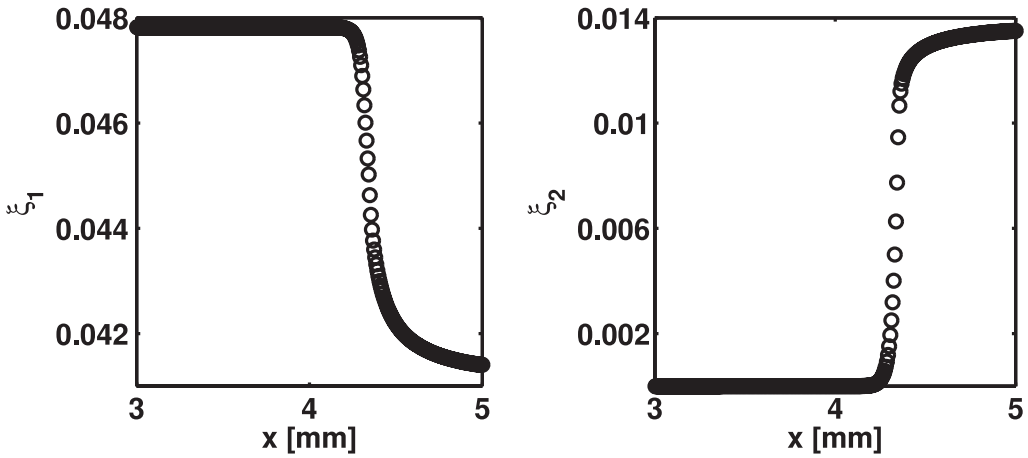

Figure 10. Manifold parameters along the channel.

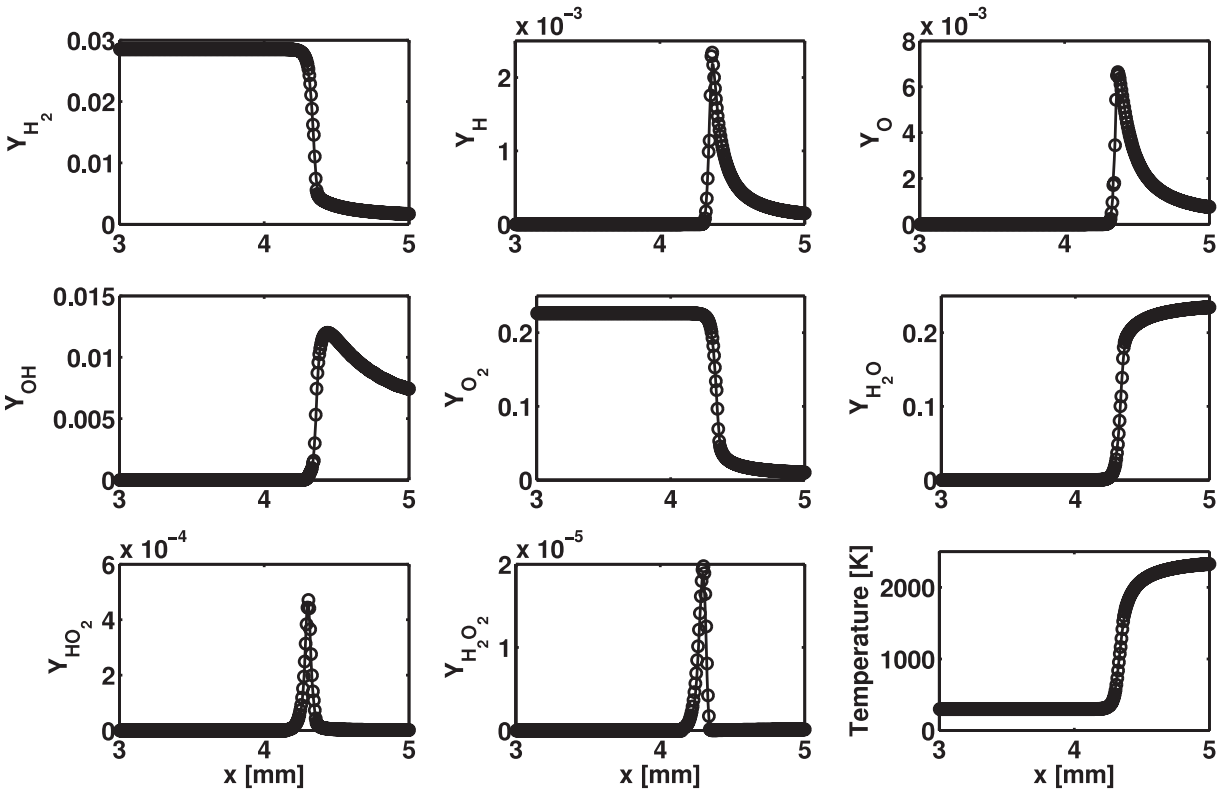

Figure 11. Detailed solution (continuous lines) versus reduced solution (circles) reconstructed with parameters of figure 10.

Here, the equilibrium populations for the reduced variables ξ^j read

$$\xi_\alpha^{j\mathrm{eq}} = w_\alpha \xi^j \left[1 + 3\,(e_\alpha v) + \tfrac{9}{2}\,(e_\alpha v)^2 - \tfrac{3}{2} v^2\right], \tag{54}$$

where $D = \Delta t(2\tau_\xi - 1)/6$, $Q_{\xi^j} = \sum_i l_i^j Q_{Y_i}$, $\xi^j = \sum_{i=1}^{9} l_i^j Y_i = \sum_{\alpha=1}^{3} \xi_\alpha^j$. Notice that $\{\boldsymbol{l}^j = (l_1^j, \ldots, l_n^j)\}$ is the set of vectors introduced for the quasi-equilibrium grid

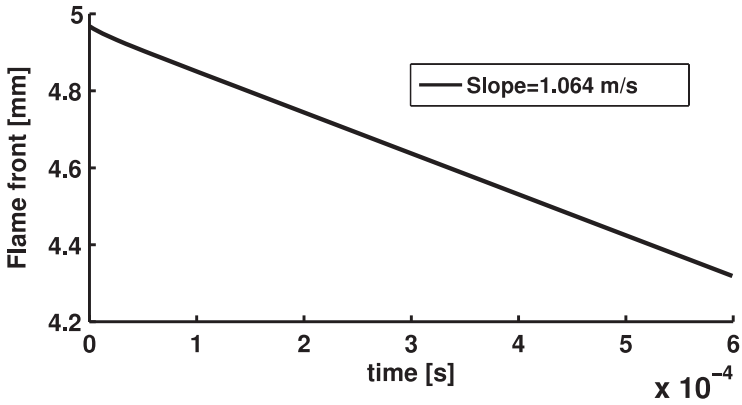

Figure 12. Flame front position versus time.

parameterization in section 4.1 and defined in section 6.1. Now, the setup of section 6.2 can be simulated by solving for only the two lumped variables ξ^j using equations (53) and tabulated source terms Q_{ξ^j}, while the flow dynamics still follows (31). The result is shown in figure 10, and all relevant fields $Y_i(\xi^1, \xi^2)$, $T(\xi^1, \xi^2)$ can be reconstructed by interpolation on the invariant grid in post-processing. Here, in the low temperature region, a 1D induction manifold is used, instead of detailed chemistry. The induction manifold is obtained by a fit from the detailed solution and it is parameterized by ξ^1. This time, due to the slow dynamics of ξ^j, computations are stable with $\Delta t \leq 1 \times 10^{-6}$: yet, as reported in figure 11, the detailed solution is reproduced with excellent accuracy. It is worth stressing that a remarkable saving, in terms of memory, is now achieved, too. Indeed, for the 1D problem presented, the number of density functions, stored at each lattice node, is one fourth. Whenever the hypothesis of equal diffusivity can be applied, such an approach is revealed to be extremely convenient, especially in the case of the larger population set needed for 2D and 3D reactive flows. Finally, in figure 12 the flame position is shown as a function of time. The flame is defined as the point with the highest heat release Q_h at a given time. The linear dependence indicates that the flame moves at constant speed given by $S_L = \text{slope} + v_{\text{in}} \cong 2.26$ m s^{-1}. The value of the burning velocity S_L is in perfect accordance with the detailed model prediction (up to 2%) and in good agreement with experimental data (see, e.g., [21]).

7. Conclusions and outlook

In this paper, we have suggested a methodology for using accurate reduced chemical kinetics in combination with a lattice Boltzmann solver for simulating reactive flows. It has been shown that the MIG is suitable for providing the reduced description of the chemistry, and this approach enables us to cope with stiffness when solving the LB species equations. This is particularly desirable in the case of explicit solvers, and it results in a remarkable speedup. Moreover, in applications where differential diffusivity effects can be neglected, the computational effort and memory demand can be drastically reduced in a very simple manner. In the near future, we plan to further investigate the performance of the technique presented for both more complex flows (2D, 3D) and more demanding fuels (e.g. simple hydrocarbon fuels such as methane).

J. Stat. Mech. (2009) P06013

Acknowledgments

This work was partially supported by SNF (Project 200021-107885/1) (EC) and CCEM-CH (IVK).

References

[1] Williams F A, 1985 *Combustion Theory* (*The Fundamental Theory of Chemically Reactive Flow Systems*) 2nd edn (Reading, MA: Addison-Wesley)
[2] Kee R J, Dixon-Lewis G, Warnatz J, Coltrin M E and Miller J A, 1996 *Report No.* SAND86-8246 Sandia National Laboratories
[3] Rockafellar R T, 1996 *Convex Analysis. Princeton Landmarks in Mathematics* (Princeton, NJ: Princeton University Press)
[4] Gorban A N and Karlin I V, *Method of invariant manifold for chemical kinetics*, 2003 *Chem. Eng. Sci.* **58** 4751
[5] Gorban A N, Karlin I V and Zinovyev A Y, *Invariant grids for reaction kinetics*, 2004 *Physica* A **333** 106
[6] Chiavazzo E, Gorban A N and Karlin I V, *Comparison of invariant manifolds for model reduction in chemical kinetics*, 2007 *Commun. Comput. Phys.* **2** 964
[7] Gorban A N and Karlin I V, 2005 *Invariant Manifolds for Physical and Chemical Kinetics* (*Springer Lect. Notes Phys.* vol 660) (Berlin: Springer)
[8] Keck J C and Gillespie D, 1971 *Combust. Flame* **17** 237
[9] Hamiroune D, Bishnu P, Metghalchi M and Keck J C, *Rate-controlled constrained-equilibrium method using constraint potentials*, 1998 *Combust. Theory Modelling* **2** 81
[10] Tang Q and Pope S B, *A more accurate projection in the rate-controlled constrained-equilibrium method for dimension reduction of combustion chemistry*, 2004 *Combust. Theory Modelling* **8** 255
[11] Chiavazzo E and Karlin I V, *Quasi-equilibrium grid algorithm: geometric construction for model reduction*, 2008 *J. Comput. Phys.* **227** 5535
[12] Chiavazzo E, Karlin I V, Frouzakis C E and Boulouchos K, *Method of invariant grid for model reduction of hydrogen combustion*, 2009 *Proc. Combust. Inst.* **32** 519
[13] Li J, Zhao Z, Kazakov A and Dryer F L, 2004 *Int. J. Chem. Kinet.* **36** 566
[14] Maas U and Pope S B, *Simplifying chemical kinetics: intrinsic low-dimensional manifolds in composition space*, 1992 *Combust. Flame* **88** 239
[15] Lam S H and Goussis D A, *The CSP method for simplifying kinetics*, 1994 *Int. J. Chem. Kinet.* **26** 461
[16] Arcidiacono S, Mantzaras J, Ansumali S, Karlin I V, Frouzakis C E and Boulouchos K, *Simulation of binary mixtures with the lattice Boltzmann method*, 2006 *Phys. Rev.* E **74** 056707
[17] Arcidiacono S, Karlin I V, Mantzaras J and Frouzakis C E, *Lattice Boltzmann model for the simulation of multicomponent mixtures*, 2007 *Phys. Rev.* E **76** 046703
[18] Prasianakis N and Karlin I V, *Lattice Boltzmann method for thermal flow simulation on standard lattices*, 2007 *Phys. Rev.* E **76** 016702
[19] Yamamoto K, He X and Doolen G D, *Simulation of Combustion Fields with Lattice Boltzmann Method*, 2002 *J. Stat. Phys.* **107** 367
[20] Chen S and Doolen G, *Lattice Boltzmann method for fluid flows*, 1998 *Annu. Rev. Fluid Mech.* **30** 329
[21] Law C K and Kwon O C, *Effects of hydrocarbon substitution on atmospheric hydrogen–air flame propagation*, 2004 *Int. J. Hydrog. Energy* **29** 867

J. Stat. Mech. (2009) P06013